AAPG Annual Meeting
March 10-13, 2002
Houston, Texas

2D/3D Geophysical Modeling of Mezozoic Onshore Rocks and Tertiary Offshore Sediments

ALLEN, LOWRIE, Consultant, Picayune, MS; EVGENII, KOZLOV, Paradigm Geophysical, Ltd, Moscow; VIKTOR, HAYDUKOV, Varyoganneftegaz, Raduzhnyi; JOEL, WATKINS, Texas A & M University, TX; IGOR, GARAGASH, Institute of the Earth's Physics, Moscow: VALENTIN, MAKAROV, Paradigm Geophysical, Ltd, Moscow; TATYANA, MALYAROVA, Paradigm Geophysical, Ltd, Moscow.

SUMMARY

2D/3D technique of geomechanical modeling combined with paleotectonic restorations is presented. It highlights spatial distribution of pore pressure and localization of intense fracturing. Implementation of the technique in West Siberia (Russia) and offshore Louisiana (USA) provided better understanding of origins of oil/gas accumulations and helped delineate productive parts of the two areas.

INTRODUCTION

Determination of spatial distribution of stress and strain components in rocks and sediments given the geologic structure and variations of elastic moduli and density is a well known (Cundall, 1988, Garagash et al., 1994) procedure of geomechanical modeling. Potentially, it can provide an additional insight into localization of zones of relative decompaction and anomalous pore pressure and lateral variations of increased permeability due to the reservoir rock fracturing for integrated reservoir characterization.

Wide industrial use of geomechanical modeling for reservoir characterization was hampered by insufficient accuracy of input data on geologic structure and elastic moduli distribution. The situation is changing with the worldwide advent of 3D seismic surveys and prestack depth migration. These routinely provide more accurate geometry of the subsurface and detailed distribution of interval velocities containing information on spatial variations of rock elastic moduli. Combining geomechanical modeling with paleotectonic restorations (Mushin et al., 2000) gave rise to paleogeomechanical restorations (Kozlov et al., 2000) – a new methodology that helps understand the evolution of reservoir properties in geologic time.

In the examples presented, 2D/3D geomechanical modeling procedures are illustrated and the relation between fracturing-induced and fracture-generating stresses and strains is discussed from the viewpoint of fracturing parameters and pore pressures. Zones of increased fracturing are described in terms of geomechanics explaining a specific *geomechanical* hydrocarbon trap.

2D/3D GEOMECHANICAL MODELING - BASIC DEFINITIONS

The new approach described here is based on the modeling of the stressed state of a porous, fluid saturated, elasto-plastic sediment or rockmass.

Input data is represented by spatial distribution of rock and sediment density and geomechanical modules deduced from the geologic structure, and a.depth velocity model resulting from prestack depth migration of seismic data.

The key idea is that real rock and sediment subjected to confining stress usually deforms as an elasto-plastic medium: after a maximum point on the stress-strain dependence is reached, deformation continues with decreasing stress until the strength limit is stabilized at a certain residual level. At first, the geologic mass deforms as an elastic body, but past the maximum of the stress-strain curve, it reacts to stress as a plastic medium.

The descending (unloading) branch of the stress-strain curve leads to rheological instability and consequent concentration of deformations in local zones. Forming of a particular pattern of fracturing depends on the distribution of internal rockmass inhomogeneities and shapes of formation boundaries, while the distribution of zones of increased fracturing is controlled by the variations of the internal friction angles, and sliding along fault surfaces results in permeability-dependent re-distribution of pore pressure.

2D/3D GEOMECHANICAL MODELING - THE PROCEDURE

The 3D geomechanical modeling aimed at the detection of zones of increased fracturing and anomalous pore pressure includes the following stages.

(1) Structure/formation analysis (Mushin et al., 1999) and sequence stratigraphy studies of seismic images built using modern prestack depth migration; structural inversion and creation of 2D/3D depth velocity models; finally, basin modeling procedures (GeoDepth Power and GeoSec software products);

(2) Paleotectonic restorations carried out using 3D GeoSec. (Usually, these first two stages are repeated iteratively to build a geologically consistent model).

(3) Geomechanical modeling conducted for contemporaneous and paleo-structure using the 2D/3D Coulomb-Mohr elastoplastic model (Cundall, 1988; Garagash et al, 1994) to calculate 2D/3D distributions of stresses and strains and their derivatives. The input data here is the depth velocity model amended by available information on lithology, strain and shear strength (cohesion) limits, dilation angles, angles of internal friction, and upper limits of the pore fluid pressure;

(4) Calculation of angles of internal friction specific to sets of fracturing being modeled and estimates of pore pressure distribution, and

(5) Integrated interpretation of the geomechanical modeling and the information on aligned fracturing derived from anisotropy measurements and AVO analysis.

EXAMPLE OF 3D GEOMECHANICAL MODELING ON A FAULTED OIL FIELD

Significant results of 3D geomechanical modeling, combined with 3D paleotectonic restorations, were obtained at the Suslikovskoye oil field in the Middle Priob'e, West Siberia, **Figure 1**. The main target here is a thin (10 to 20 m) Upper Jurassic sandstone reservoir enclosed in a bitumen rich shale. The reservoir rock had moderate porosity (0.14 to 0.17) but very high (up to a Darcy) permeability due to a system of subvertical fractures. The oil deposit is attributed to a small amplitude anticline (**Figure 1**), but only some wells drilled at the anticline are productive.

3D seismic data acquired to delineate the oil-water contact, reveal a series of subparallel small amplitude faults complicating the anticline.

Figures 2 and **3** represent cubes of, respectively, prestack depth migrated seismic data and a result of 3D geomechanical modeling – namely, average contemporaneous effective stress variations $?\tilde{?}\Sigma$, where Σ is the lithostatic plus tectonic pressure defined

as a result of horizontal averaging of the confining pressure values over each depth slice. General consistence between the cubes becomes evident in the light of additional modeling results.

In **Figure 4,** a depth slice of vertical component of the shear stress cube is shown. The slice level (= 2550 m) is chosen to lie between the Pre-Jurassic basement and the target horizon. The figure reflects the localization of main faults at this level as an alternation of narrow zones of stress and relaxation stretched along the fault tracks, compare **Figure 4** with **Figure 1**.

Rather unexpectedly, a zone of considerable compressive stress (negative stress values) is localized at the dome and west flank of the oil-bearing anticline, where several highly productive wells are located. The excessive compression should have decreased the permeability, attributed to bed boundaries with weakened cohesion (linear slip interfaces, Shoenberg, 1983), and, to a lesser degree, the reservoir rock porosity.

To resolve the apparent contradiction, calculations of subvertical fracturing intensity and pore pressure were carried out using the elasto-plastic rock model. In parallel, paleotectonic restorations and thickness analyses were carried out, and seismic attributes were calculated. Integrated interpretation of all the information allowed explanation of this apparent contradiction.

Distribution of fracturing calculated from variation of internal friction angles is shown in **Figures 5a** and **6**. The less the friction angle, the more intense the fracturing. **Figure 5a** illustrates qualitatively the fracturing intensity in the target interval block cube. The cube front section cuts the middle of the anticlinal structure in latitudinal direction. In the figure, zones of minimal friction angles (maximum fracturing) are dark, and zones of maximum friction angles (minimum fracturing) are light. As seen, the target interval is characterized by increased fracturing. Maximum fracturing within the target interval is attributed to local uplift of Pre-Jurassic basement, compare **Figures 1, 5a**, and **6**, to which the zone of increased vertical component of confining stress is attributed, **Figure 4**.

Qualitative distribution of pore pressure is shown in **Figures 5b** and **7**. Minimum pore pressure zones are dark, and maximum are light. In the pore pressure map **(Figure 7)**, minimum to maximum pressure relation is insignificant (about 0.9), while in pore pressure block cube, constructed by analogy with the fracturing intensity cube in **Figure 5a**, minimum pressure relates to maximum as 1 to 4!

The target interval is characterized by relatively high pore pressure as compared to overlaying and underlaying strata, **Figure 5b**. Within the target interval (**Figure 7**), pore pressure increases from North-East to South-West. At the uplift of the Pre-Jurassic basement (see **Figure 1**), a local minimum of pore pressure is delineated. This minimum coincides, in space, with the most productive part of the oil reservoir (see the positions of productive wells in **Figure 1**) and, roughly, with the local minimum of acoustic impedance (**Figure 8**) and maximum of fracturing intensity, **Figure 6**. Obviously, high pore pressure within the target interval had driven the hydrocarbons into the reservoir, while zones of increased fracturing provided channels for oil migration and subsequent accumulation.

2D GEOMECHANICAL MODELING IN A REGION OF COMPLEX SALT TECTONICS

The input data is a single deep seismic time section from offshore Louisiana, crossing the shelf, and terminating at mid-slope, and containing salt in the deeper section, **Figure**

9. Geomechanical modeling was aimed at revealing zones favorable for hydrocarbon accumulation from the viewpoint of the state of effective stress.

Prestack depth migration of the section revealed two distinct salt domes with a deep trough between them. The salt body top is outlined well whereas the base of salt, especially the salt “roots” under the domes, is not clear, so the interpretation presented in **Figure 10** is one of several modeled versions.

Tectonic paleorestorations for the section were carried out using GeoSec software system. The technique of balanced cross-section construction implemented in GeoSec allowed deviation from the well known principles of mass, volumes, and areas preservation to account for peculiars of salt tectonics (Rowan, 1993; Lowrie and Lerche, 2000).

The depth velocity model and its 0.4, 1.4, and 2.4 Ma paleorestorations are presented in **Figures 11** to **14.** The 2.4 Ma restoration describes a crucial moment when salt penetrated the overlaying sediments, reached the seaflor and spread over it filling the relief depressions. The 1.4 and 0.4 paleorestorations included subsidence, accumulation of fresh sediments, salt diapirism and faulting. Other possible scenarios, e.g., salt intrusion after deposition of younger sediments, is not considered here.

The present-day model and 1.4 Ma paleorestoration (**Figures 11** and **13**) were used for creation of, respectively, present-day and paleogeomechanical models. Of a number of geomechanical parameters modeled, including principal shear stress, shear strain intensity, and strain velocity variations, the most informative proved to be average confining stress variations (**Figures 15** and **16**).

The average stress variations are, in essence, the confining stress deviations from its average value calculated for a given horizontal level, **Figures 15** and **16**. Negative stress deviations (painted gray) lead to relative overcompaction; positive deviations are extensive stresses causing decompaction, promoting a favorable condition for hydrocarbon accumulation. In the sediments above salt, the most intense present-day decompaction is localized in the trough between the two salt diapirs near the flanks of the diapirs; see two brightly colored zones in **Figure 15**. In the paleo average stress variation section (**Figure 16**), these two zones are also the most decompacted. Note that paleo decompaction was more intense than in the present-day section. The stability of decompaction in these zones during the last 1.4 Ma makes them a potential exploration target. Note that the surrounding sediments are overcompacted both today and were 1.4 million years ago. If decompacted sandy layers here alternate with impermeable clays (quite common for clastic formations filling the trough), then existence of hydrocarbon traps screened by steep salt diapir flank seems to be highly probable. As to the subsalt deposits, a bright zone of decompaction is located just below the base of salt in the middle of the section (remember, position of the base of salt is uncertain!).

Distribution of principal shear stress is especially important from the viewpoint of fracturing intensity. The largest principal shear stress values are predicted for subsalt deposits in both present day and paleo sections**.** Within the salt, shear stress is relaxed, and in the sediments above the salt, the increased shear stress is concentrated near the salt body surface with maximum curvature, thus creating favorable conditions for radial fracturing adding for sediment permeability.

Distribution of shear strain intensity reflects the obvious fact that strains in salt are much larger than in surrounding clastic rocks, and that the largest strains are concentrated at the salt body flanks with maximum dip and curvature of salt body. Increased shear strain between 35 and 55 km in the deposits above salt coincides with the position of relative

decompression**.** In paleo and especially in contemporaneous sections, the most intense shear strains are concentrated in a narrow salt horizon at the base of the trough between two salt diapirs. Because of uncertainty of the base of salt, these extra-large values of strain cannot be regarded as reliably applicable to the sediments and may be related to the salt.

On the whole, patterns of paleo and contemporaneous stress and strain distributions are alike, and generally, the paleo stress and strain variations are more intense than are contemporaneous stresses and strains.

Increased paleo and contemporaneous displacement velocities, both vertical and horizontal, as should be expected, are attributed to the peaks and steep flanks of the two salt diapirs. Note that the "finger-shaped" diapir to the right of the trough, **Figures 10** to **13,** moved faster 1.4 million years ago than it did recently. As to the left diapir, the relation is reversed.

The work was partially supported by Russian Fund of Basic Researches, grants 99-05-65537 and 00-15-98580.

CONCLUSION

- The 2D/3D geomechanical modeling, combined with paleotectonic restorations, is a useful tool to help understand hydrocarbon deposits evolution and re-estimate exploration risks.
- In the area of the Suslikovskoye oil field, geomechanical modeling helps clarify the geologic history and confirms the role of subvertical fractures developed in the target reservoir rock, as main agents of increased horizontal permeability.
- When interpreting regional seismic data from offshore Louisiana, geomechanical modeling helps detect zones favorable for hydrocarbon traps. Two such zones are localized above the allochtonous salt near the steep slopes of the trough between the two salt diapirs, and a third, less reliable, at the base of salt. The decompaction regime favorable for hydrocarbon accumulation has been stable in these zones during last 1.4. Ma and probably existed long before that. Increased shear stresses and strains are also characteristic for decompacted zones in clastic sediments.
- The technique of geomechanical modeling, combined with paleotectonic restorations, is supported by the FLAC software system, Itaska, and the sequence of modern software products developed by Paradigm Geophysical, Ltd.

REFERENCES

Cundall P.A., 1988. A microcomputer program for modelling large-strain plasticity problem. Numerical methods in Geomechanics. Balkema, Rotterdam, 2101-2108.

Garagash I.A., Nikolaevsky V.N., Shatilov V.I., 1994. Connection of the deep anomalies of the crust stresses with under salt hydrocarbon deposits of the North Caspian. Proceedings of the RAS, **338**, 383- 386.

Kozlov, E.A., Garagash I.A., Makarov V.V., and Petrov A.I., 1999. Seismic-based Geomechanical Modeling. EAGE 61th Conference and Exhibition, Helsinki, P-530.

Kozlov, E.A., Garagash I.A., Mushin I A., Makarov V.V., and Lowrie A., 2000. Seismic-based Geomechanical Restorations in Volgo-Ural Region and Offshore Louisiana. EAGE 62nd Conference and Technical Exhibition, Glasgow, P-111.

Lowrie, A., and Lerche,I., 2000. Gulf's evolution - key to potential plays. The Americal Oil & Gas Reporter, April, 117 – 124.

Mushin I.A., Makarov, V.V., Kozlov E.A., and Lowrie A., 2000. Structural-Formational Interpretation Tools for Seismic Stratigraphy. Geophysical Prospecting, 48, 953-981.

Rowan,M., 1993, A systematic technique for the sequential restoration of salt structures. Tectonophysics, **228**, 331-348.

Schoenberg, M., 1983, Reflection of elastic waves from periodically stratified media with interfacial slip: *Geophys. Prospecting*, **31**, 265-292.

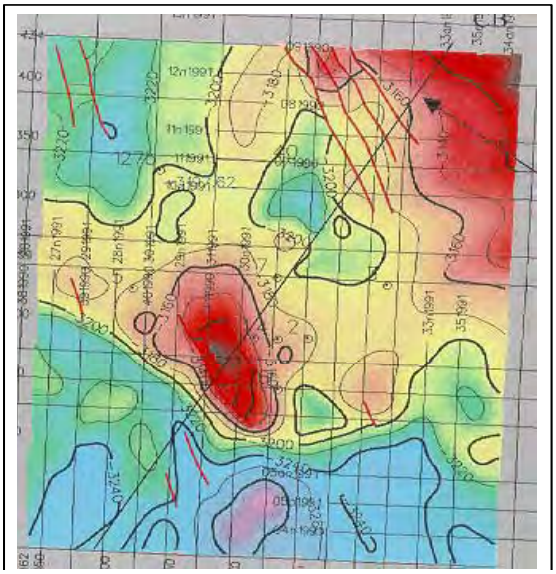

Fig. 1. Structure map of the Pre-Jurassic basement surface below the target horizon. Dotted lines are tracks of main faults. Wells 1, 2, and 6 are productive, wells 7 and 40 are not.

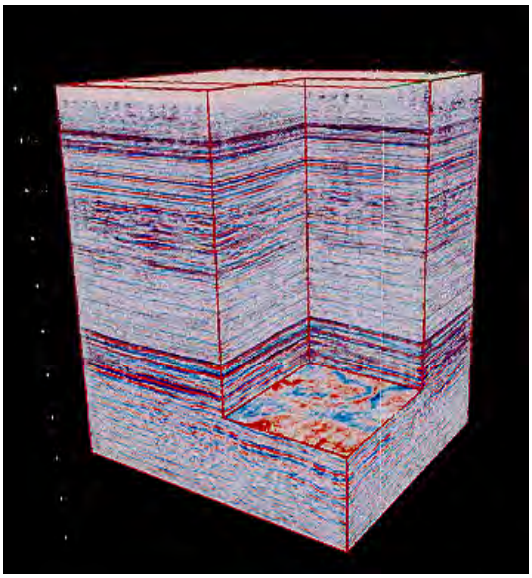

Fig. 2. Prestack depth migrated data cube

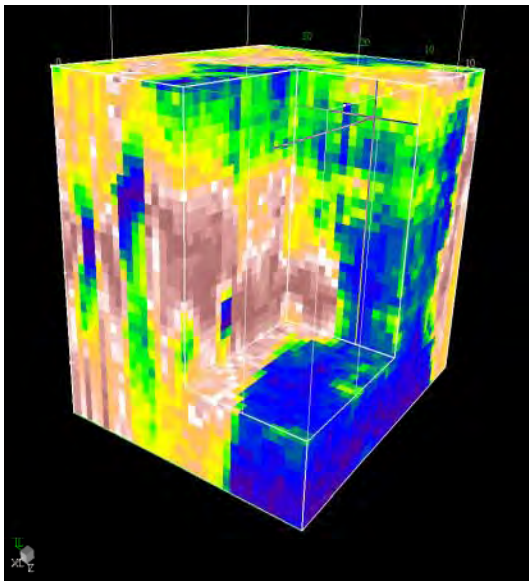

Fig. 3. Cube of average stress variations $\Delta\bar{\sigma} = \sigma - \Sigma$, where Σ is the lithostatic pressure defined as a result of horizontal averaging of the confining pressure σ values over each depth slice.

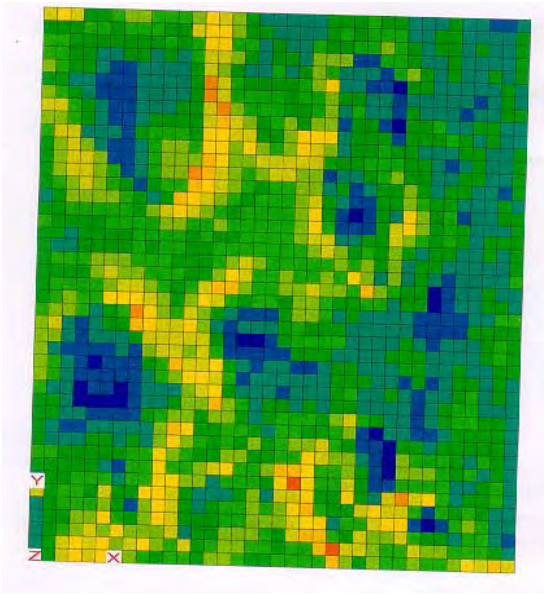

Fig. 4. Slice of volume distribution of vertical normal stress, depth = 2550 m . Dark areas are of decreased shear stress values,

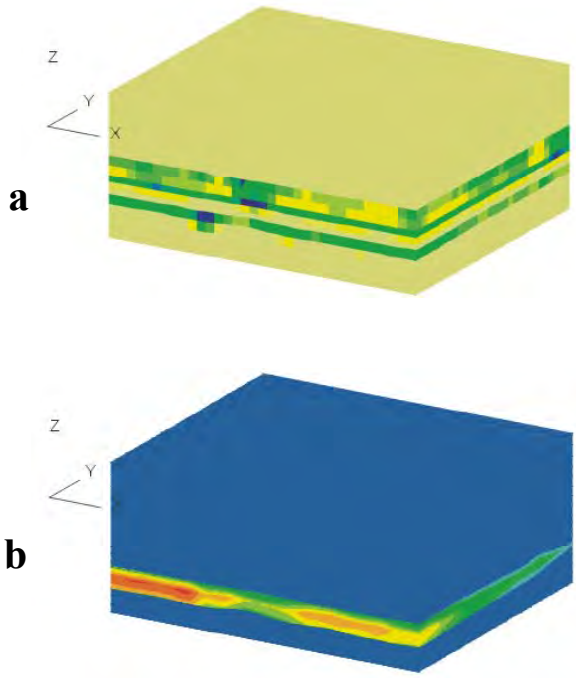

Fig. 5. Qualitative distribution of fracturing intensity (**a**) and pore pressure (**b**) in the vicinity of target interval at depths 2300 to 2400 m, latitudinal section across the basement uplift. Note relatively increased

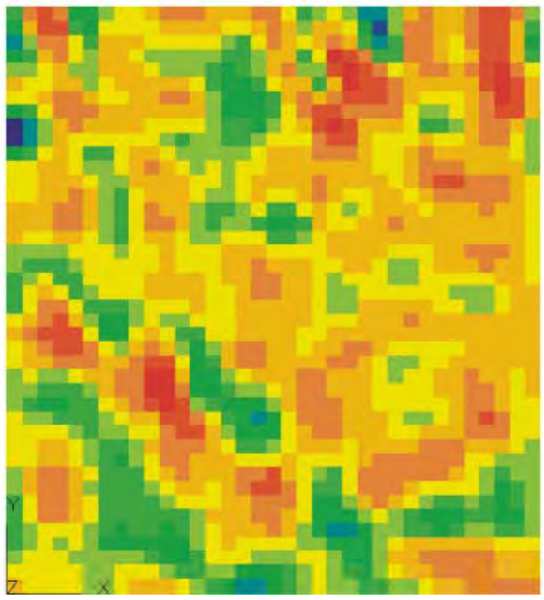

Fig. 6. Qualitative distribution of fracturing intensity at the depth of 2350 m (middle of the target interval).

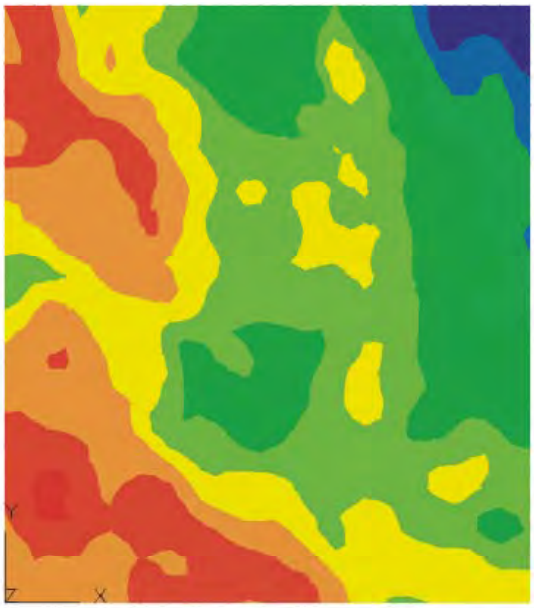

Fig. 7. Qualitative distribution of pore pressure at the depth of 2350 m (middle of the target interval).
Minimum pressure is the dark zone at the north-east corner, maximum pressures are light zones. Note pore pressure local minimum (dark) at the area of the Pre-

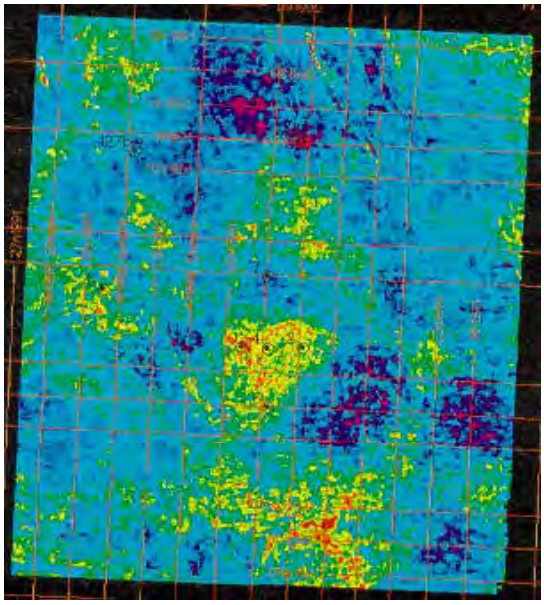

Fig. 8. Acoustic impedance within the reservoir layer. Minimum values (light) are localized at the productive part of the reservoir

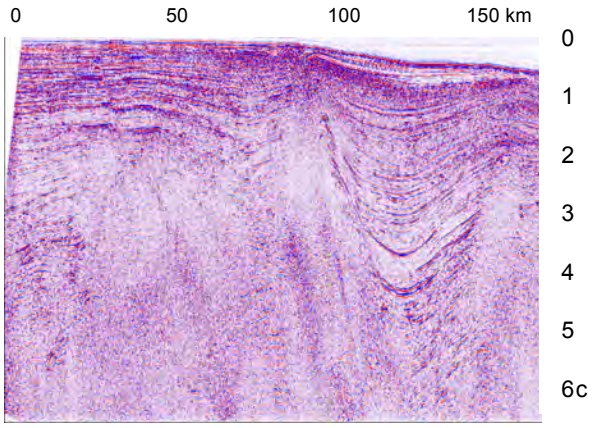

Fig. 9. Part of input time section for offshore

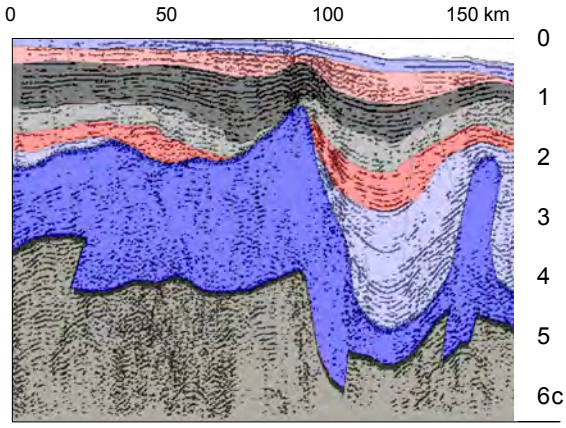

Fig. 10. Interpreted time section

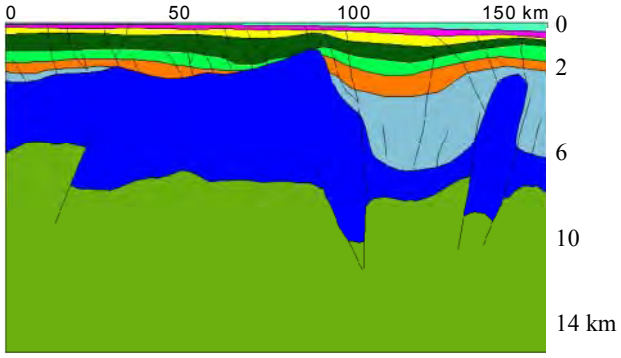

Fig. 11. Present-day depth velocity model used for geomechanical modeling

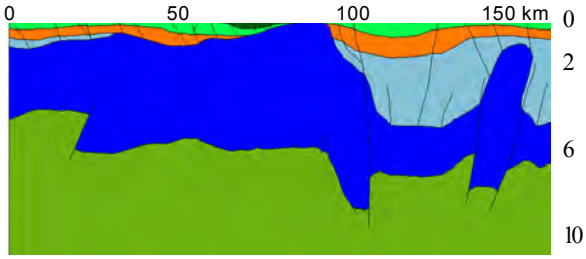

Fig. 12. Depth velocity model - 0.4 Ma paleorestoration

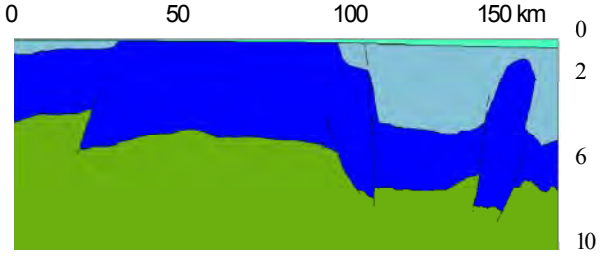

Fig. 13. Depth velocity model - 1.4 Ma paleorestoration used for paleogeomechanical modeling

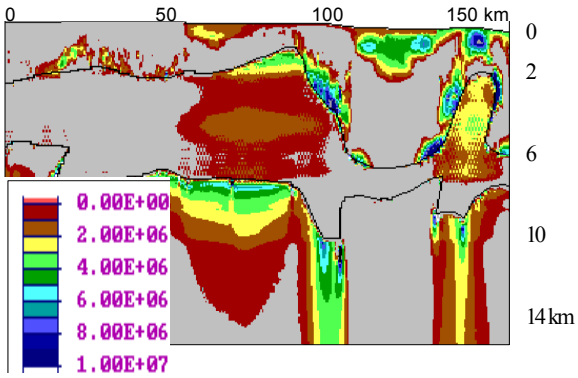

Fig. 15. Average confining stress variations (lithostatic plus tectonic stress σ minus average value of σ over a given horizontal level), present day section. In deposits above-salt, the decompaction zones (blue

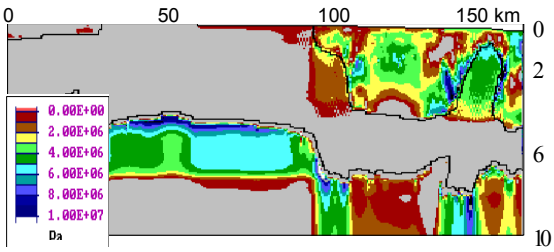

Fig. 16. Confining stress variations - 1.4 Ma geomechanical paleorestoration . Blue and green decompaction zones are more prominent than in the present-day section, see **Figure 15**.

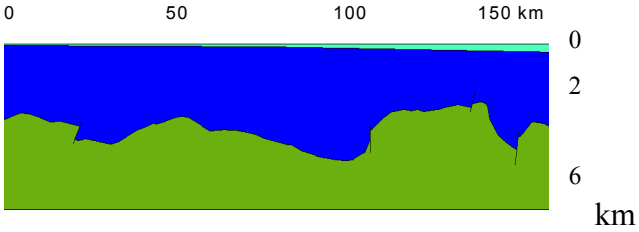

← **Fig. 14.** 2.4 Ma restored depth velocity model